

Production and knockout of nucleon isobars from helium by 5 GeV pions

S. Jonsson, S. Dahlgren, T. Ekelöf,* P. Grafström,* E. Hagberg, A. Hallgren, and S. Kullander
Gustaf Werner Institute, University of Uppsala, S-751 21 Uppsala, Sweden

B. Badefek and J. Nassalski

Institute of Experimental Physics and Nuclear Research, University of Warsaw, 00-681 Warsaw, Poland

J. Berthot, P. Cotte, C. Doré, L. Meritet, M. Querrou, and F. Vazeille

Laboratoire de Physique Corpusculaire, IN2P3, University of Clermont-Ferrand, 63170 Aubiere, France

J. P. Burq, M. Chemarin, M. Chevallier, B. Ille, and M. Lambert

Institut de Physique Nucléaire, IN2P3, University of Lyon, 69621 Villeurbanne, France

G. Fäldt*

Institute of Theoretical Physics, University of Stockholm, S-113 46 Stockholm, Sweden

P. C. Gugelot

Physics Department, University of Virginia, Charlottesville, Virginia 22901

(Received 5 April 1979)

Using both recoil and fast-particle spectrometers, the reaction $\pi^- + {}^4\text{He} \rightarrow \pi^- + {}^3\text{H} + x$ has been measured for triton momenta in the region 0.24–0.60 GeV/c. The experimental spectra are presented as functions of triton momentum and angle and of mass of the unmeasured object. In the theoretical analysis it is assumed that the final state can be reached via quasielastic scattering from $N^*{}^3\text{H}$ states and via N^* productions from the p ${}^3\text{H}$ state of helium. The most credible of three investigated p ${}^3\text{H}$ wave functions requires one percent of $N^*{}^3\text{H}$ states in the mass range 1.08–1.80 GeV/c².

NUCLEAR REACTIONS ${}^4\text{He}(\pi^-, \pi^-x)t$, $E = 5$ GeV, $E_t > 10$ MeV measured $\sigma(\theta_t, m_x)$, $\sigma(m_x, E_t)$, $\sigma(m_x, \theta_t)$; deduced p - t wave- f , x - t prob. $1.1 < m_x < 1.8$ GeV. $p(\pi^-, \pi^-)x$, $E = 5$ GeV, measured $\sigma(m_x)$.

I. INTRODUCTION

During recent years efforts have been made trying to establish the existence of non-nucleonic constituents of nuclei. Kerman and Kisslinger¹ introduced 1% of the NN^* (1688) configuration in the deuteron ground state to explain the anomalous backward peak seen in 1 GeV proton-deuteron scattering.^{2,3} Subsequent work has shown that the result can also be explained with conventional nucleon wave functions. Later, Goldhaber⁴ interpreted the slow backward $\Delta(1232)$ isobars seen in pion-deuteron interactions at 15 GeV as spectator particles from a pre-existing $\Delta\Delta$ pair in the deuteron. The final analysis⁵ gave an upper limit of 0.7% for such a pair in the deuteron. Neither in this nor in the following spectator experiments could it be ruled out that the backward Δ was produced on a nucleon or was formed by a produced pion and a spectator nucleon.⁶ The most recent Δ spectator experiment investigated proton-deuteron interactions at 19 GeV.⁷ The analysis accounted for some of the final state interactions between the spectator nucleon and the produced particles. An upper limit of $0.1 \pm 0.2\%$ for the $\Delta\Delta$ admixture was obtained.

Lately searches for Δ isobars in other reactions have been reported. The conclusions were negative for the ${}^{26}\text{Mg}(p, \pi^-){}^{27}\text{Si}$ reaction,⁸ uncertain for the ${}^2\text{H}(\pi^-, \pi^-)pn$ reaction⁹ and quite promising for the preliminary interpretation of the ${}^3\text{He}(p, t)\Delta^{**}$ reaction.¹⁰ Reviews on the subject isobars in nuclei can be found in Refs. 11 and 12.

In the present experiment we look for $N^*{}^3\text{H}$ components of helium. Only $I = \frac{1}{2}$ isobars are allowed in this configuration. The experiment was designed as a search for quasielastic pion-isobar scattering with a spectator triton.¹³ As in $(p, 2p)$ reactions the momentum distribution of the residual triton nucleus contains information on the momentum density of the initial particle before its knockout.

In order to distinguish knockout isobars from produced isobars a comparison with the elementary $\pi p \rightarrow \pi x$ reaction is of interest. Gerasimov¹⁴ proposed that a comparison between the elementary reaction and the inclusive reaction $\pi A \rightarrow \pi x$, where A is a nucleus, might give information about pre-existing isobars from an excess of cross section in the inelastic part of the mass spectrum.

The most probable isobar configuration of the helium nucleus has been found by Horlacher and

Arenhövel¹⁵ to be the ΔNNN state occurring with a probability of 2%. At 5 GeV the cross section for producing isobars on a free nucleon is a few percent of the elastic πp cross section. Hence, in an inclusive reaction on helium, pion scattering from the Δ , assumed to occur with the same strength as elastic πp scattering, is expected to give the same contribution to the mass spectrum as Δ production from the bound nucleons.

In the exclusive ${}^4\text{He}(\pi, \pi N^*){}^3\text{H}$ reaction investigated here the background production of N^* 's can be reduced considerably taking advantage of the fact that the $p^3\text{H}$ and $N^*{}^3\text{H}$ wave functions are different. Weber¹⁶ recently calculated the momentum distribution and the probability for the occurrence of $N^*{}^3\text{H}$ configurations in the ground state of helium. He found that only the N^* (1535) and N^* (1700) are present with sizable probabilities, together of the order of 0.4%. These resonances are isospin one-half, spin one-half negative parity states. The momentum density distributions peak at 0.3 GeV/c to be compared with 0.1 GeV/c for the $p^3\text{H}$ configuration. Hence, restricting the triton recoil momenta to be above 0.3 GeV/c severely reduces the background from produced N^* 's.

The first results of our experiment were analyzed using the impulse approximation. Neglecting the background and upper limit of 0.24% of the $N^*{}^3\text{H}$ state was found for N^* 's in the mass range 1.30–1.85 GeV/c² and for tritons in the momentum range 0.32–0.70 GeV/c.¹⁷

There are several background processes producing high-momentum tritons. Thus, for example a slow pion can be produced in a pion-triton interaction leaving the triton with a large recoil momentum and the slow pion and the spectator proton forming an isobarlike system. Another possibility is that the isobar is produced on a bound proton and the triton is given an additional momentum through subsequent interactions with either the pion or the produced isobar. Our theoretical formulas, developed in detail elsewhere,¹⁸ take these background processes into account. In this paper the full experimental results are presented and compared with the calculations using different $p^3\text{H}$ wave functions with and without the $N^*{}^3\text{H}$ states.

II. EXPERIMENTAL ARRANGEMENT

A. Design philosophy

The experiment was designed to measure and identify triton recoils of momenta between 0.24 and 0.60 GeV/c in a polar-angular range from 45° to 135°. Only pions scattered leftwards with angles less than 5° and momentum losses below 2 GeV/c

were accepted by the fast-particle spectrometer.

The following reactions are studied:

$$\pi^- + p \rightarrow \pi^- + x, \quad (1)$$

$$\pi^- + {}^4\text{He} \rightarrow \pi^- + {}^3\text{H} + x. \quad (2)$$

The unmeasured object x can be a proton, an isobar, or a system consisting of a nucleon and one or more mesons. Figures 1(a) and 1(b) depict the collision process in which the pion collides either with x , assumed to exist in helium, or with the triton. The hit particle receives momentum from the incident pion, while the spectator particle moves with its initial momentum isotropically distributed in space. When tritons and pions scattered to the same side are selected, the importance of the pion-triton interaction [Fig. 1(b)] is reduced and the interactions between the pion and x are enhanced.

Background produced on the proton [Fig. 1(c)] is reduced strongly by the selection of high-momentum tritons. Background arising from the pion-triton interaction [Fig. 1(d)] is not reduced in the same way by this selection; the triton receives momentum transfer from the fast pion and recoil momentum when the slow pion is emitted. When the triton and the pion both scatter leftwards, larger initial triton momenta are required minimizing this background. *A priori* tritons scattered to the left thus offer the most favorable conditions for detecting pre-existing isobars.

B. General layout of the experiment

The layout of the experiment (Fig. 2) shows the basic ingredients which are the four planes of

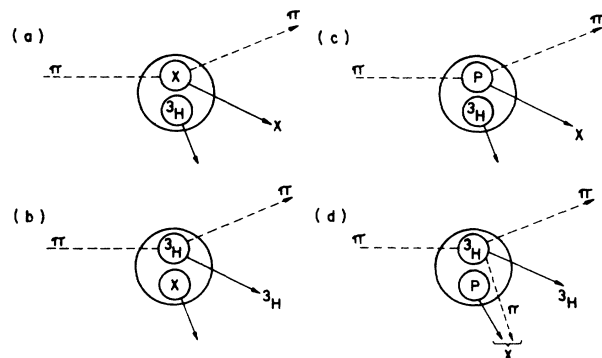


FIG. 1. Different collision processes. (a) The incident pion interacts with a pre-existing object x . The spectator triton will recoil to either side of the beam with equal probability. (b) The pion interacts with the triton. In this case the triton scatters preferentially to the opposite side of the pion. (c) The object x is produced from a proton. (d) A slow pion is produced in the pion-triton interaction simulating an object x .

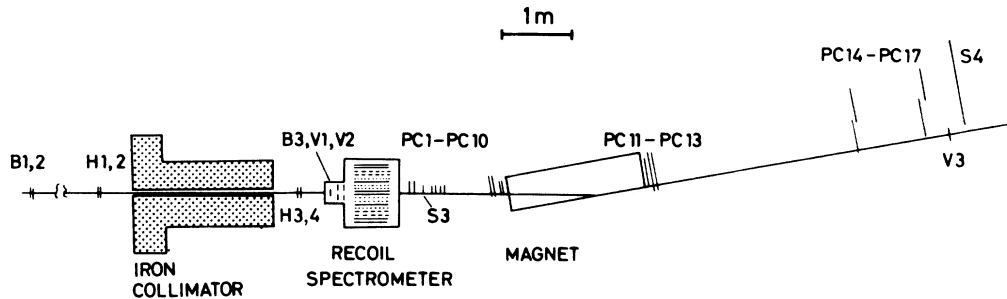


FIG. 2. Layout. The B 's and S 's are scintillation counters for the incident and scattered particles. $V1$ and $V2$ are veto counters against beam-halo particles and $V3$ is a veto-counter against unscattered beam particles. The H 's are scintillator hodoscope planes and the PC 's are MWPC planes for the tracks of the fast particles.

scintillator hodoscopes for measurement of the incident particle, the recoil spectrometer for measurement and identification of the nuclear fragment and the fast-particle spectrometer for momentum measurement of the scattered pion. A detailed description of the spectrometers and their performance has been given elsewhere.¹⁹ Below we shall only recall the most significant features.

C. Beam

A 5 GeV/ c secondary negative pion beam from the CERN PS was used. The beam contained on the average 10^6 pions per 400 ms burst every 2.4 s. The momentum bite $\Delta p/p$ was 2% and the associated momentum resolution was improved a factor of three by means of the information from two partly overlapping scintillators placed in a momentum dispersed waist of the beam. The contamination of kaons at the target position was about 1%. The 15 scintillators in each plane of the hodoscopes were 3 mm wide, determining the precision in the measurement of the direction of the beam particle. The useful part of the beam was defined by the four hodoscope planes and three scintillation counters in front of the target; thus a beam size at the target of 12 mm diameter was defined. To reduce the flux of halo particles, a 2 m long iron collimator with a 5 cm horizontal slit was placed between the two hodoscope blocks.

D. Targets

The target was gaseous and two types of containers were used. One was thin-walled with 25 μ m kapton (tradename) walls supported by a helical wire cage with 0.4 mm thick stainless steel wires and with a wire spacing of 2 mm. The diameter of the target cylinder was 2 cm and the length 50 cm. This target was normally operated at 15 atm of helium and it was used in order to obtain low-

momentum tritons. The other target container was made of titanium; it had a diameter of 2 cm, a length of 58 cm, and its walls were 0.25 mm thick. It was operated at 150 atm of helium or hydrogen.

E. Recoil spectrometer

The recoil spectrometer had two identical arms enclosed in a steel vessel and located on either side of the gas target (Fig. 3). Each arm covered an azimuthal angle of 22° . The particles emitted from the target traversed four planes of multiwire proportional chambers (MWPC's). Three of the planes, W_1 , W_2 , and W_4 , were used for the measurement of the polar angle. One plane, W_3 , together with the vertex point, gave the azimuthal angle. The recoil particles might stop in either of the two planes SC1 and SC2, each containing eight silicon semiconductor detectors about 0.25 and 0.60 mm thick respectively or it might stop in one of the scintillators S1 or S2. The kinetic energy and the nature of the particle was determined from the measured energy losses in the detectors SC1, SC2, and S1.

F. Fast particle spectrometer

The magnet used for momentum determination of the scattered pion was a CERN standard bending magnet with an active volume $2.0 \times 0.5 \times 0.2$ m³ and with a bending power of 3.0 Tm giving a 10° deflection angle for 5 GeV/ c pions. The magnet was placed unsymmetrically in such a way that only particles scattered into the left hemisphere were accepted. Thus a larger range in four-momentum transfer and in missing mass was obtained. The track in front of the magnet was determined in ten planes of MWPC's. Downstream of the magnet the pion track was measured in seven planes of MWPC's arranged in three blocks at different distances behind the magnet.

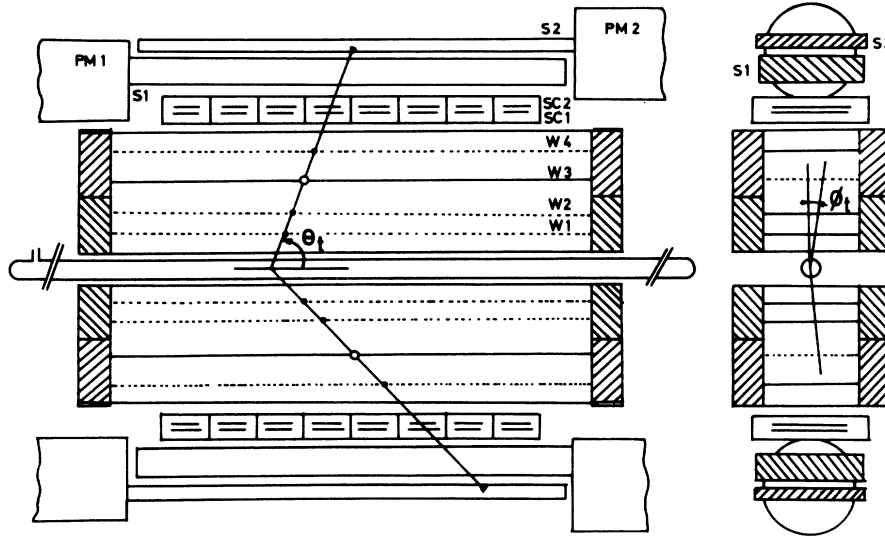


FIG. 3. Views of the recoil spectrometer cut by a horizontal plane and by a plane perpendicular to the beam. $W1$, $W2$, ($W3$), and $W4$ are MWPC's with vertical (horizontal) wires. $SC1$ and $SC2$ are the semiconductor planes with 8 detectors in each. $S1$ and $S2$ are scintillators.

G. Trigger

The signature for an interaction by the fast particle was coincidence between the signals from the scintillation counters before and after the target ($H_1H_2H_3H_4B_3\bar{V}_1\bar{V}_2S_3\bar{V}_3$). With the high-pressure target the rate of this coincidence was typically 500 per burst. The summed signal from the 16 semiconductor detectors $SC1$ turned out to be very efficient in reducing the trigger rate. When this signal was included in the trigger, the rate was reduced from 500 to about 2 per burst.

III. EVALUATION

A. Identification and energy of the recoil particle

The identification was made with two different methods depending on whether the particle stopped in a semiconductor $SC2$ or in the scintillator $S1$. In the first case the relation between the energies lost in the first and second semiconductors gave a clear identification.²⁰ In the second case the identification was more difficult because of the less accurate energy determination and the particle-dependent light-energy relation. Singly and doubly charged particles could be clearly separated but there was some ambiguity in the separation of tritons from deuterons. This ambiguity was resolved by calculating for each particle hypothesis the differences in measured energy losses in the semiconductors $SC1$ and $SC2$ and the losses calculated from the measured scintillator light. The identity corresponding to the lower χ^2 was chosen. The method was checked with Monte Carlo simulated events having their energy losses

smearred out by the observed resolutions in the three detectors. For generated events 2.5% of the deuterons were identified as tritons and 7.5% of the tritons were identified as deuterons. For measured events there were about three times as many deuterons as tritons, so the total amount of events of a given identity in the momentum range of interest is thus fairly unaffected by this ambiguity.

Particles which left the semiconductor $SC2$ and did not produce signals above the scintillator threshold were not identified. The associated loss of events in this region of triton momenta was compensated by increasing the weight (defined below) by a factor determined from the assumption of a smooth energy-loss distribution in the semiconductors of the first plane. The mean value of the correction factor was 1.5 and the maximum value was 3. This correction was applied to about 10% of the events.

The energy at the vertex was obtained by adding to the measured energy, the energies lost in the media between the points of emission and detection. The obtained energy was found to be in agreement with the energy derived from the pion scattering angle in the elastic $\pi^4\text{He} \rightarrow \pi^4\text{He}$ reaction which was also recorded in the experiment and identified by kinematical constraints. The standard error in recoil energy varies and is typically 10%.

B. Weighting

The detection probability for each measured event was determined by generating events with

the same kinematical variables but with varying beam direction, vertex point, and azimuthal angle. Each generated event was traced through the apparatus to determine if it would have been detected or not. Owing to the limited azimuthal-angle range covered by the semiconductors, events were generated only inside $\pm 11^\circ$ around the center of each recoil spectrometer arm. Up to 20 accepted events were required in a maximum of 400 generations. Thus a weight equal to the inverse of the detection probability was assigned to each event. The mean of these weights was 9, and 5% of the events had weights above 40. In the kinematical region studied, practically no events with weights higher than 25 remained.

C. Efficiencies and cross section

The efficiency of each of the recoil chambers $W1$, $W2$, and $W4$ was determined from the frequency of tracks with two coordinates as compared to the number of tracks with three coordinates. It was a function of the ionization power and angle of the recoil particle, and varied from 0.99 to 0.90. At least two hits were required to define a track, giving an efficiency always above 0.97.

The efficiencies of the wire planes in front of the magnet were typically 0.99. There were four planes with horizontal wires, four with vertical wires, and two planes had their wires inclined 45° . Since in each projection a minimum of 3 hits were required, the space-track reconstruction efficiency was 0.98. The efficiencies of the wire planes behind the magnet were typically

0.95. There were three planes with vertical wires and two planes with inclined wires. Tracks were reconstructed only in the horizontal projection and two hits were necessary to define a track yielding an efficiency of 0.99. Thus the overall detection efficiency for finding a track in the forward spectrometer was 0.97.

Table I gives the amount of events registered for the measured reactions and for the experimental background with "empty" target. For the high-pressure target events were analyzed if the recoil stopped in a semiconductor SC2 or in the scintillator S1. For the low-pressure target only events with recoils stopping in SC2 were used. The experimental background for the $\pi^4\text{He} \rightarrow \pi^3\text{Hx}$ reaction measured with 1 atm target pressure is no larger than expected from the interactions with the residual gas and the distributions of identity, mass, and angle are similar to those obtained with 150 atm helium in the target. Therefore no background subtraction was made. After correction for the inefficiencies the error in absolute normalization of the cross section scale is estimated to be $\pm 15\%$.

The performance of the two spectrometers was tested independently in measurements of elastic scattering. The recoil spectrometer was checked from the measurement of $\pi^4\text{He}$ elastic scattering.²¹ The obtained differential cross section agreed reasonably well in magnitude and shape with calculations based on multiple scattering theory.

The fast-particle spectrometer was checked from πp elastic scattering and the cross section found at zero momentum transfer was 10% below

TABLE I. Number of events registered with recoils reaching the different detectors and remaining after the analysis subdivided according to the identity.

Target and container material	Incident beam	Registered events				Remaining after analysis				
		SC1	SC2	S1	S2	p	d	t	^3He	^4He
15 atm He 0.025 mm kapton	1.7×10^{11}	206 000	54 000	41 000	18 000
						4 435	3 050	2 604	694	154
					
					
150 atm He 0.25 mm titanium	1.0×10^{11}	291 000	126 000	216 000	16 000
						20 234	13 459	7 763	1 418	108
						49 360	31 380	8 998	908	71
					
1 atm He 0.25 mm titanium	9.9×10^9	7 000	1 000	1 000
						6	4	2	0	0
						7	3	2	1	0
					
150 atm H ₂ 0.25 mm titanium	3.1×10^9	830 000					120 000			
1 atm H ₂ 0.25 mm titanium	2.7×10^9	750 000					51 000			

the optical point. The hydrogen data have therefore been normalized to the optical point, and after this correction the systematic error of the cross section is estimated to be $\pm 10\%$. The reason for the discrepancy is probably that the empty-target background (Table I) has been subtracted with some excess. As only the pions were measured, the vertex coordinates, especially the coordinate z along the beam direction, were not so well determined. The distribution of the coordinate z has two broad peaks corresponding to the end windows of the target container. The 120 000 events were selected from the central 34 cm between these peaks and the 51 000 background events were appropriately subtracted.

D. Acceptance

The variables of interest related to Eqs. (1) and (2) are k = momentum of the incident pion, k' = momentum of the scattered pion, t_{rr} = squared four-momentum transfer, ϕ_{tr} = relative azimuthal angle between the recoil triton and the scattered pion, Θ_t = polar angle of the triton with respect to the incident pion direction, p_t = momentum of the triton, m_x = missing mass.

The experimentally available range of ϕ_{tr} varies with t_{rr} as shown in Fig. 4. The two regions denoted left and right correspond to events where the tritons scattered to the left and the right sides of the beam respectively.

In Fig. 5 the events from the right arm are displayed in the $p_t \cos \Theta_t$ plane together with the limits used in the analysis. Owing to the different semiconductor thicknesses in the two arms, the lowest detectable triton momentum was 0.24 GeV/c in the left and 0.26 GeV/c in the right arm. The events to be analyzed were selected using the lim-

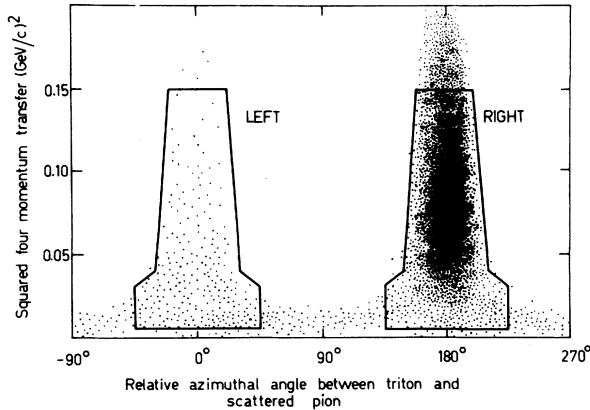


FIG. 4. Scatter plot in the ϕ_{tr}, t_{rr} plane. Only events with weight below 10 are plotted. The limits used in the analysis are superimposed.

its in Table II. The limits were adjusted to avoid high-weight events which normally occur close to the boundaries of the measured ranges.

The mass of the unmeasured object x can be calculated from the formula

$$m_x^2 = 2(m_\alpha - E_t)(E - E') + t_{rr} + t_{\alpha t} + 2\vec{p}_t(\vec{k} - \vec{k}'), \quad (3)$$

where

$$t_{\alpha t} = m_\alpha^2 + m_t^2 - 2m_\alpha E_t.$$

The maximum energy loss $E - E'$, limited by the magnet, varies from 2 to 0.7 GeV depending on t_{rr} (Table II). The last term depends on the relative angle between the triton momentum vector and the pion momentum-loss vector. Therefore the accessible missing-mass range for tritons scattered in the backward direction becomes smaller than for tritons scattered in the forward direction. In Fig. 6 the acceptance limits in the $p_t \cos \Theta_t$ plane are shown for different values of m_x and t_{rr} .

IV. EXPERIMENTAL RESULTS

A missing-mass spectrum for the $\pi p \rightarrow \pi x$ reaction is shown in Fig. 7. The level of the inelastic region lies about a factor of 25 below the elastic peak, the width of which is 53 MeV full width at half maximum (FWHM). Four isobars and a background function were used to fit the spectrum. Only the intensities and the constants in the back-

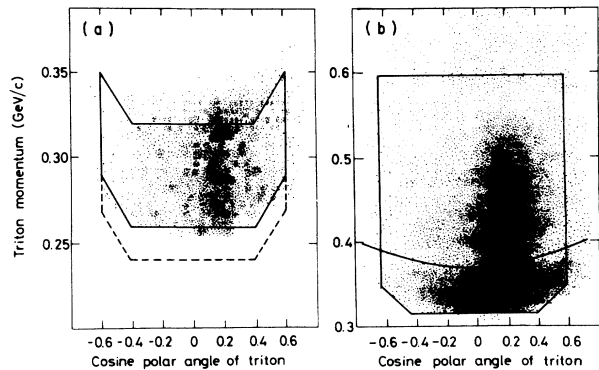


FIG. 5. Scatter plot in the $p_t \cos \Theta_t$ plane. Only events with weight below 10 are plotted. (a) Data obtained with the low-pressure target. The recoil stopped in one of the semiconductors SC2 in the right arm of the spectrometer. The limits applied in the analysis for tritons to the right are shown with full lines and the extended range for tritons to the left with dashed lines. (b) Data obtained with the high-pressure target. The recoils stopped in SC2 or S1 in the right arm of the spectrometer. The curved line indicates the upper limit for particles stopping in the semiconductors.

TABLE II. Selected ranges of variables.

Variable	Cut		Condition
	Left	Right	
$\phi_{t\pi}$ (degrees)	$ \phi_{t\pi} \leq 45$ $ \phi_{t\pi} < 93.6 - 1580t_{\pi\pi}$ $ \phi_{t\pi} < 32.0 - 77.3t_{\pi\pi}$	$ \phi_{t\pi} - 180 \leq 45$ $ \phi_{t\pi} - 180 \leq 93.6 - 1580t_{\pi\pi}$ $ \phi_{t\pi} - 180 < 32.0 - 77.3t_{\pi\pi}$	$0.005 \leq t_{\pi\pi} \leq 0.031$ $0.031 < t_{\pi\pi} < 0.040$ $0.040 < t_{\pi\pi} \leq 0.150$
P_t (GeV/c)	$0.24 \leq P_t \leq 0.32$ $0.17 \leq P_t - \cos\theta_t \times 0.167 \leq 0.25$	$0.26 \leq P_t \leq 0.32$ $0.19 \leq P_t - \cos\theta_t \times 0.167 \leq 0.25$	Low-pressure target $ \cos\theta_t \leq 0.4$ $0.4 \leq \cos\theta_t \leq 0.6$
	$0.32 \leq P_t \leq 0.60$ $0.25 \leq P_t - \cos\theta_t \times 0.167$ $P_t \leq 0.60$		High-pressure target $ \cos\theta_t < 0.4$ $0.4 < \cos\theta_t \leq 0.6$ $0.4 < \cos\theta_t \leq 0.6$
$\cos\theta_t$		$ \cos\theta_t \leq 0.6$	
$t_{\pi\pi}$ (GeV ² /c ²)		$0.005 \leq t_{\pi\pi} \leq 0.15$	
k' (GeV/c)		$k' > 2.80 + 10.3t_{\pi\pi}$, $k' > 3$	

ground function were varied. The isobars account for about half of the cross section. Table III shows the measured cross sections and the fitted slopes in four selected mass intervals. The interval 0.86–1.02 defines protons, 1.08–1.32 includes the Δ isobar, and the two regions 1.32–1.56 and 1.56–1.80 include the N^* isobars. The fitted slopes are about $9 \text{ GeV}^{-2}/c^{-2}$ except for the slope in the uppermost mass interval, which is a factor of 2 smaller. The results are in qualitative agreement with earlier measurements at 8 GeV and in a $t_{\pi\pi}$ region similar to ours.²²

The experimental cross sections for the $\pi^4\text{He} \rightarrow \pi^3\text{H}x$ reaction are presented as functions of triton polar angle and momentum for different missing-mass intervals and as functions of missing mass.

They are given in Table IV and in Figs. 8–14. Figure 8 shows the $\cos\theta_t$ distributions for the data obtained with the high-pressure target. The limits of integration are given in Table II. The cross section for quasielastic scattering defined by the mass range 0.86–1.02 is between one and two orders of magnitude larger for tritons to the right than for tritons to the left. This fact reflects, as will be seen below, the importance of the pion-triton interaction expected to be largest when the pion and the triton scatter to opposite sides of the beam. The cross sections for inelastic scattering defined by the three other mass ranges are larger and more forward peaked for tritons to the right than for tritons to the left. Figure 10 shows the p_t distributions for the data obtained from both

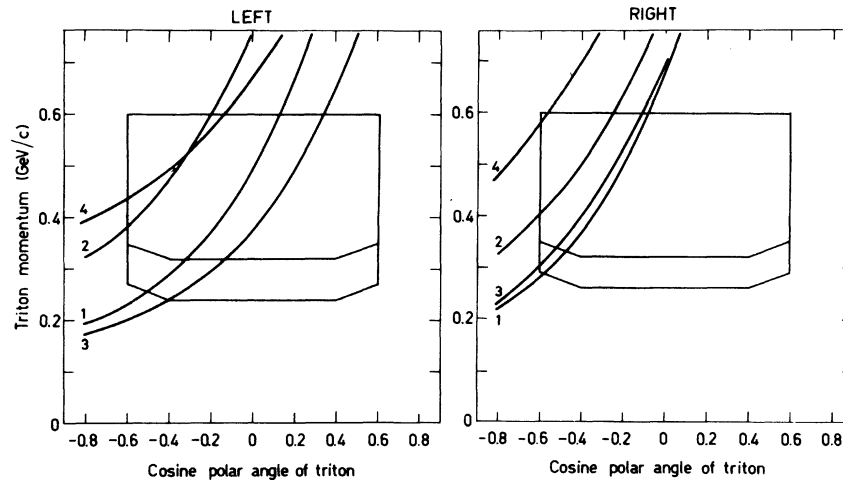


FIG. 6. Acceptance in the $p_t \cos\theta_t$ plane as a function of $t_{\pi\pi}$ and m_x . The curves show the acceptance limits for different values of $m_x/t_{\pi\pi}$: (1) 1.80/0.05, (2) 1.80/0.01, (3) 1.56/0.10, and (4) 1.32/0.10.

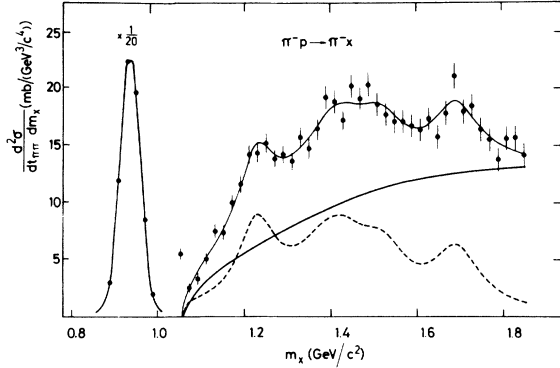


FIG. 7. Data from the $\pi p \rightarrow \pi x$ reaction with $t_{\pi\pi} = 0.005 - 0.1 \text{ GeV}^2/c^2$. The elastic peak is fitted with a Gaussian distribution of a width $53 \text{ MeV}/c^2$ (FWHM). The inelastic region is fitted by four isobars (dashed line) and a background part. The isobars are of Breit-Wigner shape, $I_r[(m_x - m_r)^2 + \Gamma_r^2/4]$. The masses m_r are 1.23, 1.41, 1.52, 1.69 GeV/c^2 and the widths Γ_r , after enlargement by the experimental resolution are 0.150, 0.206, 0.116, 0.129 GeV/c^2 . The background is taken as $a\sqrt{y} + by + cy^2$ where $y = m_x - 1.035 \text{ GeV}/c^2$. The fitted values are $I(1.23) = 0.019 \pm 0.002$, $I(1.41) = 0.079 \pm 0.013$, $I(1.52) = 0.011 \pm 0.003$, $I(1.69) = 0.020 \pm 0.005$, $a = 8.8 \pm 2.4$, $b = 17.4 \pm 8.4$, $c = -13.7 \pm 8.7$. The χ^2 for the fit is 1.16 per degree of freedom.

the low- and high-pressure targets. The cross sections are falling with increasing momentum and no pronounced structure is seen. The missing-mass spectra in Fig. 12 are subdivided according to the four directions into which the triton may be scattered. No pronounced structure except the proton peak is seen in these spectra. The level of the inelastic cross section for tritons to the left is about three times lower than the proton peak. The corresponding ratio for the $\pi p \rightarrow \pi x$ reaction was 25.

The impulse approximation is obviously not valid and in the following section formulas for inelastic scattering will be developed, which take into account also the multiple scattering and the final-state interactions between the participating particles.

V. THEORETICAL MODEL

The basic assumption in the theoretical analysis is that the initial helium nucleus can be described as a proton-triton system with a relative wave function $\psi(\vec{p})$ and in addition a small fraction described as an isobar-triton system with a relative wave function $\psi_*(\vec{p})$. In this picture the final state of reaction (2) can be reached through three separate mechanisms,

- (i) production of the system x by the proton (amplitude F_p),
- (ii) coherent production of slow pions by the triton which together with the spectator proton forms the system x (amplitude F_t),
- (iii) knockout of a pre-existing N^* (amplitude F_*).

The three amplitudes do *not* add incoherently. However, a determination of the correct relative phases would require a complete angular momentum decomposition of the final state. In reality this is an impossible task and, furthermore, the underlying nucleonic amplitudes are not sufficiently well known. We therefore add the three processes incoherently and get the approximate formula

$$\frac{d^6\sigma}{d\Omega dm_x d^3p_t} = \frac{k'}{k} (|F_p|^2 + |F_t|^2 + |F_*|^2), \quad (4)$$

where Ω is the scattering angle of the pion and k and k' are the momenta of the incident and scattered pion. This procedure can in part be justified *a posteriori* since it turns out that the main contribution comes from the proton amplitude F_p . The triton amplitude F_t is important only for small missing masses. Similarly, pre-existing N^* 's are restricted to S11 pion-nucleon states¹⁶ and consequently the F_* amplitude adds coherently only to a small part of the F_p amplitude. From the obtained results it follows that we do not expect any serious errors by adding F_* and F_p incoherently. The kinematical factor k'/k is approximate and valid in our triton recoil momentum range. The full details are given elsewhere.¹⁸

TABLE III. Measured cross sections (microbarn) and fitted slopes (GeV^{-2}/c^{-2}) in four selected mass intervals for the $\pi p \rightarrow \pi x$ reaction.

$t_{\pi\pi}$ (GeV^2/c^2) \ m_x (GeV/c^2)	0.86–1.02	1.08–1.32	1.32–1.56	1.56–1.80
0.005–0.040	1240 \pm 7	116 \pm 5	191 \pm 5	164 \pm 5
0.04–0.10	1420 \pm 8	131 \pm 4	216 \pm 6	223 \pm 6
	Slope			
0.005–0.100	8.5 \pm 0.2	9.7 \pm 0.3	8.5 \pm 0.2	3.8 \pm 0.4

TABLE IV. Measured cross sections (microbarn). Only the outer limits of integration are indicated. For details see Table II.

ϕ_{tr}	P_t (GeV/c)	$\cos\theta_t$	$m_x = 0.86-1.02$ (GeV/c ²)	$m_x = 1.08-1.32$ (GeV/c ²)	$m_x = 1.32-1.56$ (GeV/c ²)	$m_x = 1.56-1.80$ (GeV/c ²)
Left -45/45	0.24/0.35	Forward 0/0.6	0.70 ± 0.18	0.76 ± 0.20	0.73 ± 0.18	0.92 ± 0.19
		Backward -0.6/0	0.52 ± 0.15	0.34 ± 0.13	0.36 ± 0.12	0.31 ± 0.12
	0.32/0.60	Forward 0/0.6	0.57 ± 0.06	0.32 ± 0.04	0.41 ± 0.05	0.60 ± 0.06
		Backward -0.6/0	0.43 ± 0.05	0.28 ± 0.04	0.28 ± 0.04	0.25 ± 0.04
Right 135/225	0.26/0.35	Forward 0/0.6	23.31 ± 0.88	2.73 ± 0.32	1.16 ± 0.21	0.90 ± 0.19
		Backward -0.6/0	9.05 ± 0.5	0.45 ± 0.12	0.54 ± 0.15	0.34 ± 0.12
	0.32/0.60	Forward 0/0.6	34.87 ± 0.44	3.05 ± 0.14	2.37 ± 0.13	1.21 ± 0.09
		Backward -0.6/0	6.50 ± 0.20	0.82 ± 0.07	0.63 ± 0.06	0.45 ± 0.05

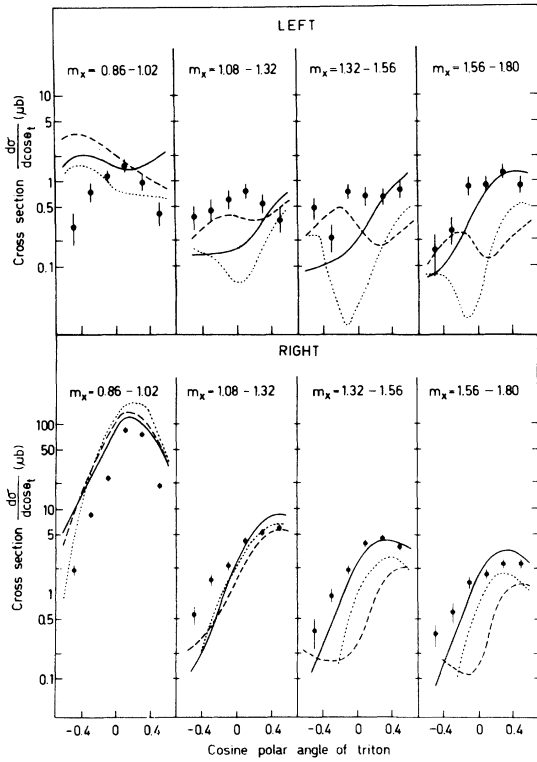


FIG. 8. $\cos\theta_t$ distributions with data obtained from the high-pressure target. The limits of integration are given in Table II. The curves are calculated from the theory using Lesniak —, Hulthén ---, and modified Hulthén ··· proton-triton wave functions.

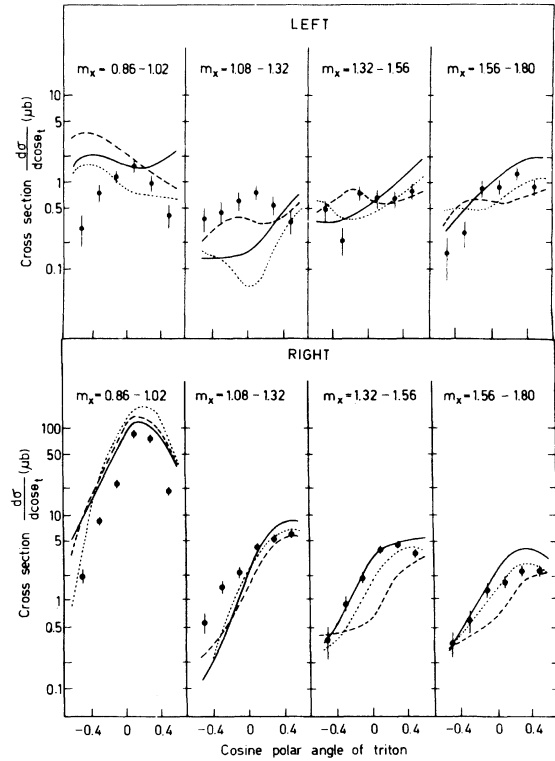


FIG. 9. $\cos\theta_t$ distributions with N^*3H wave functions added into the theory. The contributions are 0.4% each of the $N^*(1535)^3H$ and $N^*(1700)^3H$ states. The other parameters are as for Fig. 8.

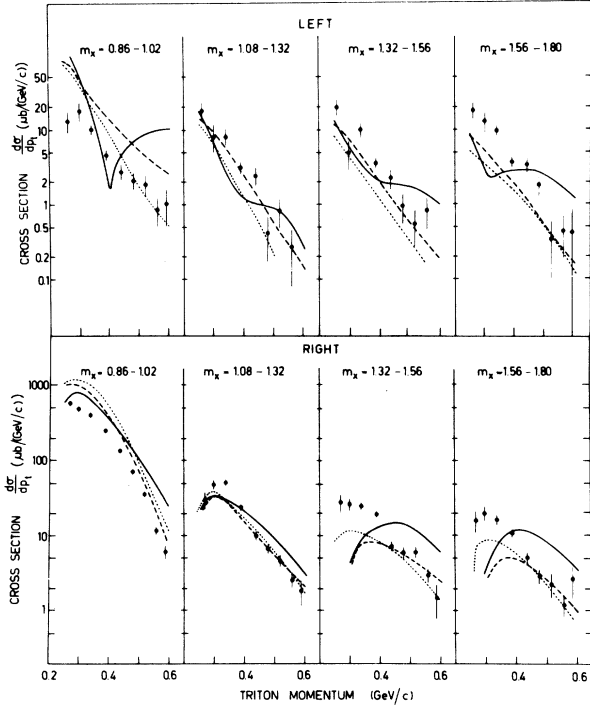


FIG. 10. p_t distributions. The data are from the two targets used and the limits of integration are given in Table II. The three different $p^3\text{H}$ wave functions are Lesniak —, Hulthén --- and modified Hulthén ···.

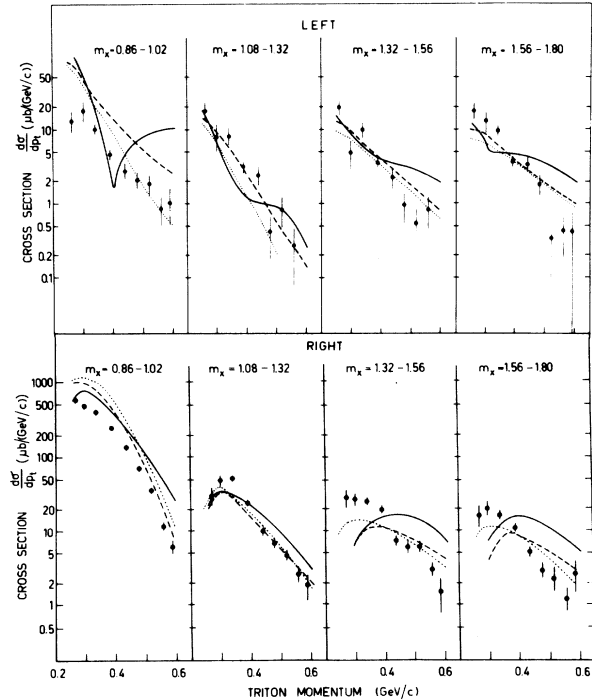


FIG. 11. p_t distributions with the $N^*{}^3\text{H}$ wave functions added into the theory. The other parameters are as for Fig. 10.

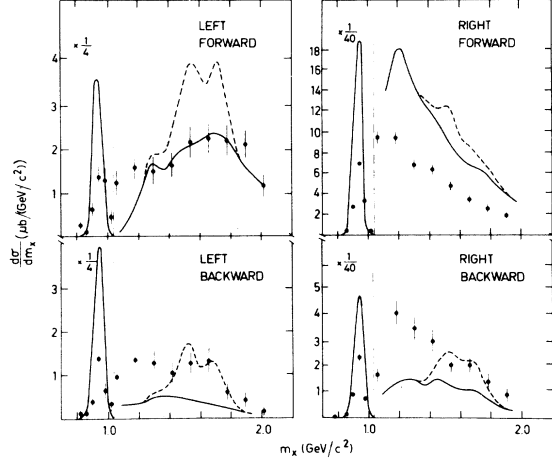


FIG. 12. Missing-mass spectra obtained with data from the high-pressure target. The calculated distributions shown with solid lines are obtained with the Lesniak wave function. The dashed lines show the distributions with the $N^*(1535)^3\text{H}$ and the $N^*(1700)^3\text{H}$ states added.

A. Production by the proton

The most obvious contribution is the impulse approximation term described in Fig. 15(a). The corresponding amplitude is given by

$$F_p^{(1)} = \psi(\bar{p}_t) f_{pr}(m_x, \bar{\Delta}_1), \quad (5)$$

where $\bar{\Delta} = \bar{k} - \bar{k}'$ and where the orthogonal component $\bar{\Delta}_1$ is the component of $\bar{\Delta}$ orthogonal to \bar{k} , i.e., $\bar{k} \cdot \bar{\Delta}_1 = 0$. The elementary $\pi N \rightarrow \pi X$ production amplitude is normalized according to

$$\frac{d^3\sigma}{d\Omega dm_x} = \frac{k'}{k} |f_{pr}(m_x, \bar{\Delta}_1)|^2 \quad (6)$$

and obtained from our measurement of the $\pi p \rightarrow \pi X$

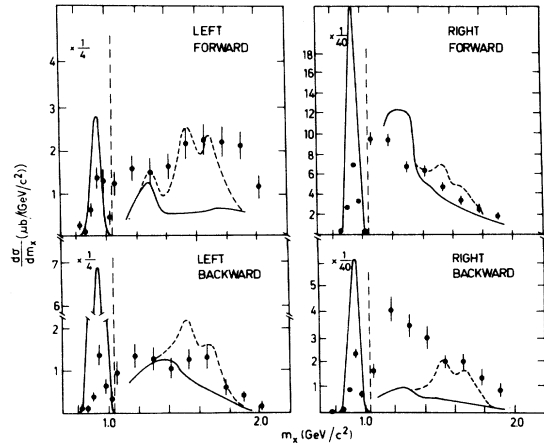


FIG. 13. Same as Fig. 12 but with the Hulthén wave function.

$$F_p^{(l)} = -\frac{1}{8\pi i \bar{p}_x^L} f_{pr}(m_x, \bar{\Delta}_1) \times \int d^2 \Delta'_1 \psi(\bar{p}_t - \bar{\Delta}'_1) f_{xt}(\bar{\Delta}'_1); \quad (10)$$

$l=4$ or 5 and \bar{p}_x^L is the relative $x^3\text{H}$ momentum. Only small $\bar{\Delta}_1$ contribute to the integral because of the f_{xt} amplitude. The amplitude of Eq. (7) is formally twice as large as that of Eq. (10), since we have twice as many diagrams in the double scattering as in the final state interaction.

The definition of the axis defining the longitudinal component of $\bar{\Delta}'$ depends on which particles are put on their mass shells. The $l=4$ amplitude is the one where the intermediate triton and x are on their mass shells. In the energy conservation law at the $x^3\text{H}$ vertex, i.e., in the equation $E_t(\bar{p}_t) + E_x(\bar{p}_x) = E_t(\bar{p}_t - \bar{\Delta}') + E_x(\bar{p}_x + \bar{\Delta}')$, we make a linear approximation in the intermediate $\bar{\Delta}'$. This equation then defines the longitudinal axis

$$\bar{\Delta}'_1(\bar{v}_x - \bar{v}_t) = 0, \quad (11)$$

where \bar{v}_x and \bar{v}_t are respectively the velocities of the final system x and the triton. We also get $\Delta'_1 \approx 0$. As $|\bar{\Delta}'|$ thus is small, it follows that the argument in the wave function in Eq. (10) is close to \bar{p}_t .

For $l=5$, the proton and x are on their mass shells. From the energy conservation law at the production vertex we get (making again a linear approximation in $\bar{\Delta}'$)

$$\bar{\Delta}'_1[\bar{v}_x + \bar{v}_p(\bar{p}_t)] = 0, \quad (12)$$

where $\bar{v}_p(\bar{p}_t)$ is the velocity of a proton of momentum \bar{p}_t . The longitudinal transfer is

$$\Delta'_1 \approx \frac{T_t(\bar{p}_t) + B_p + T_p(\bar{p}_t)}{|\bar{v}_x + \bar{v}_p(\bar{p}_t)|}, \quad (13)$$

where T_t and T_p are the triton and proton kinetic energies at the indicated momenta. Since Δ'_1 is quite large it follows that the effective momentum in the wave function can be substantially smaller than $|\bar{p}_t|$ implying a large wave function probability. Hence, we expect the $l=5$ part of the final state interaction to be particularly important.

B. Production by the triton

This background arises from pion production at the triton vertex [Fig. 15(e)]. Together with the spectator nucleon the pion forms a system of mass m_x . For the moment we assume that a single slow pion is produced in a collision with a single nucleon in the triton. Furthermore, the $N\pi$ system is treated as an independent two-particle system, the nucleon being trapped by the triton and the pion emerging from it. This picture is

different from that for the production on the proton, where we assume that the produced $N\pi$ system is a single entity as long as it is within the nucleus. Before emerging from the triton the slow pion can rescatter but we have found this effect to be negligible. On the other hand, the rescattering of the fast pion, within the triton, is important and is taken into account. Rescattering of either the slow pion, the fast pion, or the triton on the spectator proton has been calculated and found to be small. Therefore we neglect these processes.

The momentum transfer to the triton is given by $\bar{k} - \bar{k}' - \bar{p}_\tau = \bar{p}_p + \bar{p}_t$ where \bar{p}_τ is the momentum of the slow pion. When the production takes place without rescattering [Fig. 15(e)] this is also the momentum transfer to the nucleon inside the triton. When rescattering is included the orthogonal component of this transfer can change in the multiple scattering process, but the longitudinal component is always fixed and determined by energy conservation. Let us consider the single step process above. We then get the overall production amplitude

$$\bar{F}_t = N f_{pr}(\bar{m}_x, \bar{\Delta}_1) S_t(\bar{p}_t + \bar{p}_p) \psi(\bar{p}_p), \quad (14)$$

where S_t is the triton form factor. The factor N is an isospin factor which depends on the isospin structure of the nucleonic production amplitude. It will be discussed below. The mass \bar{m}_x is the mass of the $N\pi$ system produced in the triton. It is not a well defined quantity. For simplicity we set \bar{m}_x equal to the invariant mass m_x of the pion spectator-proton system. We have also investigated more sophisticated definitions of m_x assuming e.g. that the hit nucleon has an initial momentum $-\bar{p}_p/3$ and a final momentum $\bar{p}_t + 2/3\bar{p}_p$. However, these more refined definitions produced changes which are too small to be of interest for the present experiment. In the impulse approximation the production cross section is therefore

$$\frac{d^6\sigma_t}{d\Omega dm_x d^3p} \approx N^2 \frac{k'}{k} F |f_{pr}(m_x, \bar{\Delta}_1)|^2, \quad (15)$$

where the function F describes the triton dynamics and the kinematic restriction on the slow pion spectator-proton system

$$F = \frac{m_x}{\pi p_c} \int \frac{d^3p_p}{2E_p} \frac{d^3p_x}{2E_x} \delta^{(4)}(p_x - p_p - p_\tau) \times |\psi(\bar{p}_p) S_t(\bar{p}_t + \bar{p}_p)|^2 \quad (16)$$

with $E_x = (m_x^2 + \bar{p}_x^2)^{1/2}$ and p_c being the proton momentum in the proton-pion c.m. system. The integration is relativistically invariant and is evaluated by going over to the pion-proton c.m. system

$$F = \frac{1}{4\pi} \int d\Omega_c |\psi(\bar{p}_p) S_t(\bar{p}_t + \bar{p}_p)|^2, \quad (17)$$

where $\bar{p}_p = \bar{p}_p(\Omega_c, \bar{p}_x)$. Therefore, in the approximations made to this point the cross section for production by the triton is obtained from that of the proton through multiplication by a function $F(\Omega, \bar{p}_t, m_x)$ and an isospin factor.

The rescattering of the fast pion inside the triton is easily taken into account by standard Glauber methods. The expression $f_{pr}(m_x, \bar{\Delta}_1) S_t(\bar{p}_t + \bar{p}_p)$ in Eq. (14) is the single-scattering term. We do not give the explicit expression for the remaining terms in the Glauber series. They were calculated assuming a Gaussian triton wave function and taking the c.m. correlation into account exactly.

When several slow pions are produced the pion mass in F is replaced by the relevant invariant mass of the many-pion system. It is impossible to make a satisfactory treatment of this contribution since the corresponding mass distributions for production on a free nucleon are not known. We have therefore considered this effect in a simplified manner taking an effective mass of 400 MeV for the continuum and varying the relative weight of one- and two-pion contributions. These simplifications do not affect our final conclusions since the triton contribution is most important for small masses where we know that single pion production is the dominant channel.

Finally we discuss the isospin factor N^2 in Eq. (15). Its value depends on the isospin structure of the elementary nucleonic amplitude, which we use as input. For production on a free nucleon the produced $N\pi$ system has isospin $T_f = \frac{1}{2}$ or $\frac{3}{2}$. For *diffractive production* the exchanged isospin (in the t channel) is $T=0$ and the isospin of the slow $N\pi$ system is therefore $T_f = \frac{1}{2}$. The diffractive production amplitude is for a free nucleon proportional to $\bar{T}_t \bar{T}$, where \bar{T}_t and \bar{T} are the isospin operators for the slow pion and the nucleon, respectively. Let us then consider a nuclear (triton or helion) target. In the impulse approximation the nuclear amplitude becomes proportional to $\bar{T}_t(\bar{T}(1) + \bar{T}(2) + \bar{T}(3)) = \bar{T}_t \bar{T}_A$, where \bar{T}_A is the nuclear isospin operator. But the triton and the helion form an isospin doublet with $T = \frac{1}{2}$ just as the proton-neutron doublet. Consequently for pure $T=0$ exchange we get $N^2 = 1$ and *no* enhancement factor even though we have three possible nucleons to interact with. Unfortunately this simple result is not directly applicable. At 5 GeV we have a substantial *nondiffractive* component in the Δ mass range, which proceeds via $T=1$ exchange. Assume for simplicity a pure $T=1$ exchange leading to a pure $T_f = \frac{3}{2}$ final state in the nucleonic case. After some calculations we

then find for the nuclear amplitudes

$$\begin{aligned} |M[\pi^- {}^3\text{H} \rightarrow \pi^- ({}^3\text{H}\pi^0)]|^2 &= 6 |M[\pi^- p \rightarrow \pi^- (N\pi)^+]|^2, \\ |M[\pi^- {}^3\text{He} \rightarrow \pi^- ({}^3\text{H}\pi^+)]|^2 &= \frac{1}{3} |M[\pi^- p \rightarrow \pi^- (N\pi)^+]|^2, \end{aligned} \quad (18)$$

i.e., for $T=1$ exchange the ${}^3\text{H}$ nucleus acts coherently yielding a strongly enhanced nuclear production. Fortunately the production amplitude is completely known for a free nucleon. The relevant reduced matrix elements as well as their relative phases have been determined experimentally.²³ This information allows us to determine the production amplitude for a free triton including $T=0$ and $T=1$ exchanges. A detailed calculation shows that $N^2 \approx 3$ in the Δ mass region defined by the range 1.08–1.32 GeV/ c^2 , whereas for higher masses $N^2 \approx 1$.

C. Pre-existing isobars

The calculation of the contribution from the pre-existing isobars is easy since we expect the relative isobar-triton wave function to have its main strength in the region of measured triton momenta. This is quite different from production by the proton where only a small part of the proton-triton wave function remains (cf. Sec. V A). It was thus mandatory to include successive interactions originating in the momentum region where the proton-triton wave function has its main strength. For the case of pre-existing isobars on the other hand final state interactions and multiple-scattering contributions are less important. The main contributions come from the two single-scattering diagrams. $F_*^{(1)}$ in Fig. 15(f) is the amplitude for quasielastic knockout of N^* and $F_*^{(2)}$ in Fig. 15(g) is the amplitude for quasielastic knockout of the triton. The cross section is

$$\frac{d^6\sigma_*}{d\Omega dm_x d^3p_t} \approx \frac{k'}{k} |F_*^{(1)} + F_*^{(2)}|^2 \quad (19)$$

and the amplitudes are

$$\begin{aligned} F_*^{(1)} &= \psi_*(m_x, \bar{p}_t) f_{\pi x}(\bar{\Delta}_1), \\ F_*^{(2)} &= \psi_*(m_x, \bar{p}_x) f_{\pi t}(\bar{\Delta}_1). \end{aligned} \quad (20)$$

Both pion scatterings are off-shell. We have followed general practice approximating these amplitudes by the on-shell elastic amplitudes evaluated at the actual orthogonal momentum transfer $\bar{\Delta}_1$. We thus ignore the large longitudinal momentum loss of the pion. This assumption could of course be questioned and is bothersome especially for the pion-triton scattering. The correct procedure is, however, unknown. A discussion of these ambiguities can be found in Ref. 24. Furthermore, we assume the pion-isobar elastic amplitude to be equal to the pion-nucleon elastic amplitude and

TABLE V. The strengths of the different processes expressed in nanobarn for the ranges $p_t = 0.32\text{--}0.60$ GeV/c and $m_x = 1.32\text{--}1.56$ GeV/c². The subscripts $a\text{--}k$ define the type of diagram (Fig. 15). The subscript p gives the summed background from production by the proton. The subscript asterisk gives the summed interaction with the isobar-triton state. The superscript denotes which internal particle is off the mass shell, 1 for the proton and 2 for the triton. The proton-triton wave function is of the modified Hulthén type. The isobar-triton wave functions are as calculated by Weber (Ref. 16), 0.4% each of the $N^*(1535)^3\text{H}$ and $N^*(1700)^3\text{H}$ states.

Triton direction		σ_a	σ_{bc}^1	σ_{bc}^2	σ_d^1	σ_d^2	σ_f	σ_g	σ_{hi}	σ_k	$\sigma_e(=\sigma_t)$	σ_p	σ_*
Left	Forward	520	48	87	20	90	286	34	18	5	80	80	243
	Backward	510	48	10	10	3	270	2	1	4	3	85	156
Right	Forward	420	147	280	32	420	275	210	114	5	180	1170	444
	Backward	400	137	20	12	30	260	7	4	5	20	90	176

calculate the pion-triton amplitude using the Glauber theory.

We have also included double scattering and final state interactions in a way similar to that given in Sec. V A. The contributions of the individual terms as well as their coherent sum are given in Table V and their definitions are shown in Fig. 15. (For more details see Fäldt and Chevallier, Ref. 18.) We conclude that direct knockout of the isobar is by far the most important process. Taking into account the higher-order terms gives an overall reduction of the cross section. In the backward hemisphere the reduction is roughly a factor of 2, but smaller in the forward hemisphere.

The initial wave function $\psi_*(m_x, \vec{p})$ depends on a continuous mass variable m_x . In the present day N^* industry one usually considers the resonant part of the mass spectrum and approximates the resonance by a particle of definite mass. In a calculation along these lines Weber¹⁶ finds that the main contribution comes from the $N^*(1535)$ and $N^*(1700)$ isobars with probabilities of 0.4% each. His result is 0.2% of the single nucleon probability. In the theory presented here the probability is normalized with respect to the $p^3\text{H}$ cluster wave function. Since these resonances have unnatural parity, the relative isobar-triton wave function has angular momentum one, suppressing the poorly known short-range part of the wave function. The widths of each of the resonances are taken to be 100 MeV/c² represented by Breit-Wigner distributions, and the radial shapes of the wave functions as calculated by Weber.

VI. DISCUSSION AND CONCLUSION

A. The proton-triton wave function

In the present experiment we study certain aspects of the internal nucleonic structure of the helium nucleus, which have not previously been investigated. In the direct-interaction picture, knowledge of this structure is needed for relative proton-triton momenta between 0.24 and 0.60

GeV/c. This region has not been directly studied before. The $(p, 2p)$ experiments give information on momentum components below 0.2 GeV/c where the impulse approximation can be applied. At higher momenta final state interactions are expected to be important as shown by Alberi *et al.*²⁵ for the $Xd \rightarrow YNN$ reaction. The only information on the wave function is indirect and comes from an analysis by Lesniak *et al.*²⁶ of backward proton-helium scattering. In the exchange picture this reaction is dominated by triton exchange. They assume the helium nucleus to be a bound proton-triton system with a relative wave function $\psi(\vec{p})$. The wave function is determined in an *ad hoc* way by fitting the electromagnetic form factor of helium inserting the known form factors of the proton and the triton. The resulting wave function is

$$\psi_L(\vec{p}) = A \sum_{m=0}^4 (-1)^m \binom{4}{m} \frac{1}{p^2 + (\alpha + m\beta)^2} \quad (21)$$

with $\alpha = 0.846$ fm⁻¹ and $\beta = 1.42$ fm⁻¹. It changes sign at $p \approx 0.41$ GeV/c. This model gives a reasonable description of backward proton-helium scattering, and the investigated momentum region of the proton-triton wave function is similar to the one investigated in our experiment.

Our experiment, particularly the quasielastic scattering, is expected to be more sensitive to the details of the proton-triton function than elastic proton-helium scattering. Quasielastic scattering defined by the mass range 0.86–1.02 GeV/c² is analyzed in detail elsewhere²⁷ where the importance of the final-state interaction is shown. The p_t distributions calculated using the formulas in Ref. 27 and the Lesniak function lie above the experimental distributions both for left and right scattered tritons (Fig. 10). From the result for left tritons we conclude that a wave function which changes sign in the measured p_t region seems unlikely.

The sign question is connected with the short-range behavior of the coordinate space wave function. If $\psi(\vec{r}=0) = 0$ then $\psi(\vec{p})$ must change sign.

This is the case for a two-body wave function and reflects the presence of a hard core. The proton-triton wave function, however, is a cluster wave function obtained by averaging over the positions of the three nucleons in the triton. This procedure gives a soft short-range behavior of the force in coordinate space and no compelling reason to require $\psi(\vec{r}=0)=0$. Thus, in addition to the Lesniak wave function we use two phenomenological wave functions which are everywhere positive, the Hulthén wave function

$$\psi_H(\vec{p}) = \frac{A}{(p^2 + \alpha^2)(p^2 + \beta^2)} \quad (22)$$

with $\alpha = 0.846 \text{ fm}^{-1}$, $\beta = 0.940 \text{ fm}^{-1}$ and a modified Hulthén wave function

$$\psi_{MH}(\vec{p}) = \frac{A}{(p^2 + \alpha^2)(p^2 + \beta^2)(p^2 + \gamma^2)} \quad (23)$$

with $\alpha = 0.846 \text{ fm}^{-1}$, $\beta = 1.16 \text{ fm}^{-1}$ and $\gamma = 1.66 \text{ fm}^{-1}$. For all three wave functions α is determined from the binding energy. In (22) and (23) the remaining parameters are such that the maximum of $p^2 |\psi(\vec{p})|^2$ is at $|\vec{p}| \approx 100 \text{ MeV}/c$ as for the Lesniak function. Another important quantity is the probability P for the relative momentum \vec{p} to be in the region $0.3 < |\vec{p}| < 0.6 \text{ GeV}/c$. We have

$$P_L = 1.9\%, \quad (24a)$$

$$P_H = 5.8\%, \quad (24b)$$

$$P_{MH} = 2.4\%. \quad (24c)$$

The Hulthén function gives in our opinion too large a probability in the momentum region of interest. The additional constant γ in the modified Hulthén function makes it possible to attenuate the high-momentum components to a more likely value.

The result for quasielastic scattering in Figs. 8–14 shows that the three wave functions predict larger cross sections than measured. For tritons to the left the modified Hulthén function gives cross sections which are in closer agreement with the experimental result than any of the two other functions. Also the shapes of the p_t distributions are fairly well reproduced with this function. The shape of the $\cos\theta_t$ distribution for tritons to the left can, however, not be well predicted. Part of the found discrepancy might be due to the final-state interaction which is more difficult to handle for quasielastic scattering than for production. On the basis of these results we think that the modified Hulthén function is the most credible of the investigated functions.

B. Isobar production

To demonstrate the relative importance of background from production on the proton and on the

triton these separate contributions have been calculated in the $\cos\theta_t$ representation of the cross section (Fig. 16). Contrary to quasielastic scattering these distributions are strongly forward peaked much more so than the contribution from the knock-out of isobars also shown for comparison. Meson production by the triton is particularly pronounced for tritons to the right and for missing masses in the Δ range due to the enhancement coming from the isospin factor N^2 . In the left backward hemisphere production by the triton is less important than production by the proton. Numerical values of the different background processes contributing to the reaction cross section (Fig. 15) as well as their coherent sums are given in Table V. As can be seen the cross section due to interactions with the isobar-triton states (σ_*) is larger than the one from the background processes ($\sigma_p + \sigma_t$) except in

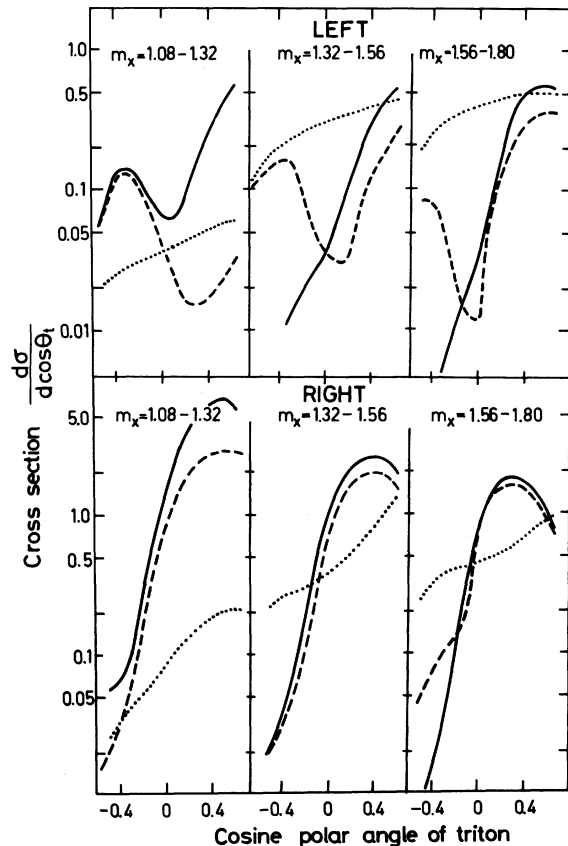


FIG. 16. Partial cross sections versus $\cos\theta_t$ calculated from the theory. The limits of integration are for the high-pressure target given in Table II. The pion-triton interaction is shown with full lines, the pion-proton interaction with dashed lines, and the interaction with the pre-existing isobar-triton state is dotted. The $p^3\text{H}$ wave function is of the modified Hulthén type and the $N^*{}^3\text{H}$ wave functions as calculated by Weber, Ref. 16.

the right forward direction. The dependence of the background on the proton-triton wave function is given in Table VI.

Figure 8 shows the summed background in the $\cos\theta_t$ representation calculated for each of the three wave functions. None of them give good agreement with the experiment. The most significant conclusion drawn from the p_t distributions in Fig. 10 is that the calculated results based on the Lesniak function is out of phase with the measured distributions particularly in the right geometry. This conclusion is not altered by including contributions from knockout of pre-existing isobars (Fig. 11). None of the three wave functions reproduce the inelastic parts of the mass spectra (Figs. 12-14). The calculation based on the Lesniak function agrees with the measured mass spectrum

only in the left forward quadrant. The Hulthén function is adequate in the right forward and left backward quadrants, whereas the modified Hulthén function is good only for the right forward quadrant. The experimental result is thus not fitted by using only conventional nucleonic wave functions.

C. Pre-existing isobars

The magnitudes and shapes of the experimental and theoretical $\cos\theta_t$ and p_t distributions in the two upper mass bins agree better when the $N^*(1535)^3\text{H}$ and the $N^*(1700)^3\text{H}$ states are added with 0.4% probability each (Figs. 9 and 11). This improvement is particularly pronounced in the $\cos\theta_t$ distribution for tritons to the left.

TABLE VI. Calculated cross sections (microbarn). The limits of integration are as for Table IV. The used $p^3\text{H}$ wave function is Lesniak (first line), Hulthén (second line), and modified Hulthén (third line). In the fourth line the contribution to the cross section from 0.4% each of $N^*(1535)^3\text{H}$ and $N^*(1700)^3\text{H}$ configurations is given.

ϕ_t	P_t (GeV/c)	$\cos\theta_t$	$m_x=0.86-1.02$ (GeV/c ²)	$m_x=1.08-1.32$ (GeV/c ²)	$m_x=1.32-1.56$ (GeV/c ²)	$m_x=1.56-1.80$ (GeV/c ²)
Left -45/45	0.24/0.35	Forward	2.6	0.47	0.23	0.17
		0/0.6	1.75	0.48	0.22	0.16
			1.4	0.35	0.17	0.15
				0.01	0.09	0.12
		Backward	5.2	0.55	0.61	0.34
		-0.6/0	3.6	0.54	0.61	0.35
	0.32/0.60		3.0	0.36	0.40	0.22
				0.01	0.07	0.10
		Forward	1.1	0.25	0.47	0.57
		0/0.6	0.85	0.21	0.14	0.14
			0.44	0.13	0.16	0.22
				0.02	0.25	0.31
Right 135/225	0.26/0.35	Backward	1.2	0.08	0.11	0.07
		-0.6/0	2.1	0.21	0.28	0.13
			0.86	0.07	0.09	0.04
				0.02	0.16	0.19
		Forward	30.1	1.90	0.50	0.33
		0/0.6	49.0	1.71	0.35	0.21
	0.32/0.60		57.0	1.95	0.50	0.35
				0.02	0.12	0.14
		Backward	15.3	0.32	0.19	0.16
		-0.6/0	21.5	0.26	0.16	0.10
			21.5	0.23	0.10	0.08
				0.01	0.08	0.11
Right 135/225	0.32/0.60	Forward	55.6	4.00	2.37	1.85
		0/0.6	67.0	2.78	1.05	0.71
			84.0	3.06	1.35	0.97
				0.10	0.45	0.40
		Backward	14.0	0.36	0.30	0.26
		-0.6/0	18.0	0.23	0.12	0.09
	0.26/0.35		16.0	0.19	0.11	0.09
				0.02	0.18	0.22

The calculated missing-mass spectra (Figs. 12–14) in the region above $1.4 \text{ GeV}/c^2$ are closer to the measured ones when the contributions from the two $N^*{}^3\text{H}$ states are added. In the backward direction the agreement between theory and experiment is substantially improved independent of the nucleonic wave function used for the background estimate. The excess of the experimental cross section in the mass region below $1.4 \text{ GeV}/c^2$ remains to be explained.

The conclusion from the analysis of the mass spectra is that our experiment gives evidence for pre-existing isobars also below $1.4 \text{ GeV}/c^2$, although it is known that the $\Delta(1232)^3\text{H}$ configuration is not allowed. One way to understand the result is to assume that the nonresonant part of the pion-nucleon S_{11} wave can also exist and be knocked out. An alternative explanation might be that the interaction between the pion and a virtual isobar results in a final isobar mass which is spread all over the mass spectrum.²⁴ The notation N^* will in the following define any object with isospin half in the range $1.08\text{--}1.80 \text{ GeV}/c^2$.

The fraction of pre-existing $N^*{}^3\text{H}$ objects is estimated using the cross sections in Table IV for left backward tritons in the range $p_t = 0.32\text{--}0.60 \text{ GeV}/c$ and $m_x = 1.08\text{--}1.80 \text{ GeV}/c^2$. After subtraction of the background obtained with the modified Hulthén function (Table VI) the cross section due to knockout N^* 's remain. The probability as a function of mass is then extracted by using the formulas in Sec. V C. Integration over the range $m_x = 1.08\text{--}1.80 \text{ GeV}/c^2$ results in a probability of 1% of $N^*{}^3\text{H}$ states with respect to the $p^3\text{H}$ state.

Calculations have been made in order to see how the mass distributions in the other three quadrants are influenced by 1% of $N^*{}^3\text{H}$ states uniformly distributed from $1.08\text{--}1.80 \text{ GeV}/c^2$. The result added to the background obtained with the modified Hulthén function shows improved agreement in three of the four quadrants as compared to the case when $N^*{}^3\text{H}$ states are absent (Fig. 14).

The theory does not work so well for tritons scattered into the right forward direction. This

discrepancy can probably be attributed to the uncertainty connected with the pion-triton interaction, which accounts for most of the cross section in this region of the phase space, particularly for masses below $1.3 \text{ GeV}/c^2$.

D. Conclusion

The most likely proton-triton momentum wave function is one which does not change sign in the momentum region considered. The modified Hulthén function used is found to give the most reasonable agreement with quasielastic scattering.

Using this wave function, isobar production is calculated and found to be smaller than what is measured in the mass region $1.08\text{--}1.80 \text{ GeV}/c^2$. By adding the contribution from interactions with the pre-existing $N^*(1535)^3\text{H}$ and $N^*(1700)^3\text{H}$ states the theory is brought into better agreement with the experiment in the mass region where these isobars are present. This mechanism cannot explain the experimental result in the mass region below $1.4 \text{ GeV}/c^2$. Owing to the absence of structure in the experimental mass spectra, a common explanation of the low and high mass regions seems likely. Two possible interpretations are that either nonresonant components x are present in the wave function or that pre-existing isobars due to large off-shell effects are knocked out with a mass different from that of the resonance. The experimental result is then explained by about 1% of such $x^3\text{H}$ components with respect to the $p^3\text{H}$ wave functions (Fig. 14).

ACKNOWLEDGMENTS

The experiment was financially supported by the Conseil National de la Recherche Scientifique, France, Swedish National Science Research Council and the Polish Ministry for Science and Higher Education. We would like to acknowledge the valuable technical support given at our home institutes and at CERN. We thank the staff of the CERN PS for providing excellent working conditions.

*Present address: CERN, 1211 Geneva 23, Switzerland.

¹A. K. Kerman and L. S. Kisslinger, *Phys. Rev.* **180**, 1483 (1969).

²G. W. Bennet, J. L. Friedes, H. Palevsky, R. J. Sutter, G. J. Igo, W. D. Simpson, G. C. Phillips, R. L. Stearns, and D. M. Corley, *Phys. Rev. Lett.* **19**, 387 (1967).

³J. S. Vincent, K. W. Roberts, E. T. Boschitz, L. S. Kisslinger, K. Gotow, P. C. Gugelot, C. F. Pedrisat, L. W. Swenson, and J. R. Priest, *Phys. Rev. Lett.* **24**,

236 (1970).

⁴M. Goldhaber, in *Proceedings of the International Conference on Nuclear Physics, Munich, 1973*, edited by J. de Boer and H. J. Mang (North-Holland, Amsterdam, 1973), Vol. II, p. 13.

⁵C. P. Horne, S. Hagopian, V. Hagopian, N. D. Pewitt, P. K. Williams, B. Wind, J. R. Bensinger, F. C. Porter, G. P. Yost, H. H. Bingham, W. B. Fretter, W. R. Graves, P. Harris, H. J. Lubatti, K. Moriyasu, W. J. Podolsky, A. Firestone, G. Goldhaber, and

- M. Goldhaber, *Phys. Rev. Lett.* **33**, 380 (1974).
- ⁶P. Benz and P. Söding, *Phys. Lett.* **52B**, 367 (1974).
- ⁷V. Bakken, H. Gennow, P. Lundborg, J. Mäkelä, M. Pimiä, B. Sellden, and E. Sundel, *Phys. Scripta* **19**, 491 (1979).
- ⁸B. Höistad, T. Johansson, and O. Jonsson, *Phys. Lett.* **73B**, 123 (1978).
- ⁹R. Beurtey, J. C. Duchazeaubeneix, H. H. Duhm, J. C. Favire, J. C. Lugol, J. Saudinos, L. Goldzahl, G. Cvijanovich, L. Dubal, and C. F. Perdrisat, *Phys. Lett.* **61B**, 409 (1976).
- ¹⁰B. Tatischeff, I. Brissaud, R. Frascaria, M. Morlet, F. Reide, R. Beurtey, A. Boudard, J. L. Escudié, M. Garcon, L. Schecter, J. P. Tabet, and Y. Terrien, *Phys. Lett.* **77B**, 254 (1978).
- ¹¹A. M. Green, *Rep. Prog. Phys.* **39**, 1109 (1976).
- ¹²H. J. Weber and H. Arenhövel, *Phys. Rep.* **36C**, 27 (1978).
- ¹³B. Badelek, J. Berthot, J. P. Burq, M. Chemarin, M. Chevallier, S. Dahlgren, T. Ekelöf, G. Fäldt, J. Gardes, P. Grafström, E. Hagberg, B. Ille, Z. Kulka, S. Kullander, M. Lambert, J. P. Martin, L. Meritet, J. Nassalski, M. Querrou, and F. Vazeille, Report No. CERN/EEC-74/41.
- ¹⁴S. B. Gerasimov, *Zh. Eksp. Teor. Fiz. Pis'ma Red.* **14**, 385 (1971) [*JETP Lett.* **14**, 260 (1971)].
- ¹⁵G. Horlacher and H. Arenhövel, *Lett. Nuovo Cimento* **18**, 503 (1977).
- ¹⁶H. J. Weber, *Phys. Lett.* **80B**, 232 (1978).
- ¹⁷B. Badelek, J. Berthot, J. P. Burq, M. Chemarin, M. Chevallier, P. Cotte, S. Dahlgren, T. Ekelöf, P. Grafström, P. C. Gugelot, E. Hagberg, A. Hallgren, B. Ille, S. Jonsson, S. Kullander, M. Lambert, L. Meritet, J. Nassalski, M. Querrou, and F. Vazeille, *Nucl. Instrum. Methods* **155**, 61 (1978).
- ¹⁸G. Fäldt and M. Chevallier, unpublished; M. Chevallier, thesis, Lyon, 1979.
- ¹⁹B. Badelek, J. Berthot, J. P. Burq, M. Chemarin, M. Chevallier, P. Cotte, C. Doré, C. Douhet, S. Dahlgren, T. Ekelöf, P. Grafström, W. Gajewski, E. Hagberg, A. Hallgren, B. Ille, S. Jonsson, S. Kullander, M. Lambert, J. P. Martin, S. Maury, L. Meritet, J. Nassalski, M. Querrou, and F. Vazeille, *Nucl. Instrum. Methods* **155**, 61 (1978).
- ²⁰F. S. Goulding, D. A. Landis, J. Cerny, and R. H. Pehl, *Nucl. Instrum. Methods* **31**, 1 (1964).
- ²¹S. Jonsson *et al.*, (unpublished); A. Hallgren, thesis, Uppsala, 1979.
- ²²E. W. Anderson, E. J. Bleser, H. R. Blieden, G. B. Collins, D. Garelick, J. Menes, F. Turkot, D. Birnbaum, R. M. Edelstein, N. C. Hien, T. J. McMahon, J. F. Mucci, and J. S. Russ, *Phys. Rev. Lett.* **25**, 699 (1970).
- ²³G. Berlad, B. Haber, M. F. Hodous, R. I. Hulsizer, V. Kistiakowsky, A. Levy, I. A. Pless, P. A. Singer, J. Wolfson, and R. K. Yamamoto, *Nucl. Phys.* **B75**, 93 (1974).
- ²⁴A. S. Goldhaber, *Nucl. Phys.* **A294**, 293 (1978).
- ²⁵G. Alberi, M. A. Gregorio, and Z. D. Thome, *Nuovo Cimento* **19A**, 586 (1974).
- ²⁶H. Lesniak, L. Lesniak, and A. Tekou, *Nucl. Phys.* **A267**, 503 (1976).
- ²⁷S. Jonsson *et al.*, (unpublished); M. Chevallier, thesis, Lyon, 1979.

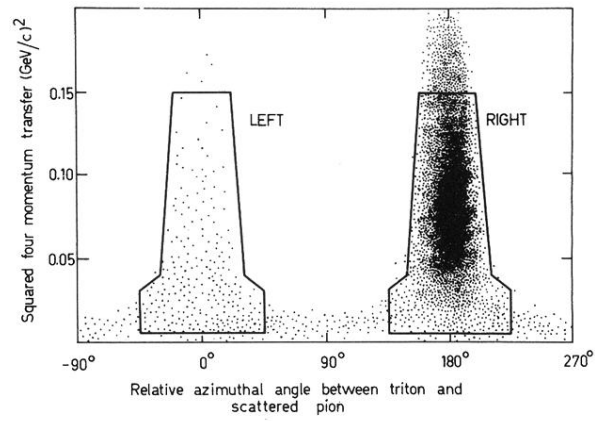


FIG. 4. Scatter plot in the $\phi_{t\pi}t_{\pi\pi}$ plane. Only events with weight below 10 are plotted. The limits used in the analysis are superimposed.

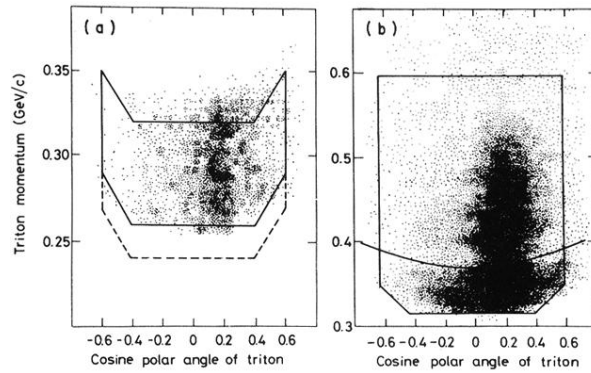


FIG. 5. Scatter plot in the $p_t \cos \theta_t$ plane. Only events with weight below 10 are plotted. (a) Data obtained with the low-pressure target. The recoil stopped in one of the semiconductors SC2 in the right arm of the spectrometer. The limits applied in the analysis for tritons to the right are shown with full lines and the extended range for tritons to the left with dashed lines. (b) Data obtained with the high-pressure target. The recoils stopped in SC2 or S1 in the right arm of the spectrometer. The curved line indicates the upper limit for particles stopping in the semiconductors.